Nafar Dastgerdi, J.; Miettinen, Arttu; Parkkonen, J.; Remes, H.

Multiscale microstructural characterization of particulate-reinforced composite with non-destructive X-ray micro- and nanotomography

Published in:
Composite Structures

DOI:
10.1016/j.compstruct.2018.04.022

Published: 15/06/2018

Document Version
Peer-reviewed accepted author manuscript, also known as Final accepted manuscript or Post-print

Multiscale microstructural characterization of particulate-reinforced composite with non-destructive X-ray micro- and nanotomography

J. Nafar Dastgerdi[a,b], A. Miettinen[c], J. Parkkonen[c], H. Remes[a]

[a] Department of Mechanical Engineering, School of Engineering, Aalto University, P.O. Box 14300, FIN-00076 Aalto, Finland

[b] Department of Aerospace Engineering, Amirkabir University of Technology, 424 Hafez Avenue, Tehran, Iran

[c] Department of Physics, University of Jyvaskyla, P.O. Box 35, FIN-40014 Jyvaskyla, Finland

* Corresponding author (Jairan.nafardastgerdi@aalto.fi)

Abstract

Methods based on X-ray tomography are developed to study the relevant statistical quantities describing the microstructural inhomogeneity of particulate reinforced composites. The developed methods are applied in estimating microstructural inhomogeneity parameters of composites containing metallic glass particles in metal matrix, extruded in varying pressure loads. This study indicates that the critical characteristics with regard to the effect of particle clustering are cluster size and shape, local volume fraction of particles in the cluster and the distance between clusters. The results demonstrate that the spatial distribution of reinforcement is very uneven and the amount of particle clustering varies with amount of reinforcement. Moreover, X-ray nanotomography was used to investigate the structure of individual clusters and the results suggest that high extrusion load may cause break-up of

individual particle clusters so that their shape changes from solid and spherical to broken and ellipsoidal.

Keywords: Particle-reinforcement, Microstructural analysis, Non-destructive testing, Multiscale

1. Introduction

Particulate reinforced lightweight metal matrix composites (MMCs) are widely used in a spectrum of engineering applications for example in aerospace and automotive industries. Conventionally, ceramic materials such as SiC and Al_2O_3 have been used as reinforcements in MMCs [1-4]. Recent research has led to utilizing metallic particles stronger and stiffer than the matrix such as Ti, Cr, and Nb, as reinforcements, to improve the strength and / or ductility without compromising lightweight [5-8]. Amongst metallic materials, amorphous alloys possess excellent properties such as extremely high strength (1 to 2 GPa), large elastic strain limit of ~2% and superior corrosion resistance, and therefore investigations on making composites reinforced with these unique materials are being performed [9-12].

In most particulate reinforced composites, the particles are not uniformly distributed. Instead, these materials contain local regions where the particles are clustered. Agglomeration of the reinforcement phase has been shown to have deleterious effects on tensile strength and flow stress [13-15], ductility [16] and fatigue performance [17-19]. Clearly, particle clustering is a serious obstacle to the commercial structural application of particulate reinforced MMC materials. Therefore, further understanding of the relationship between the processing, the structure, and the properties of particulate reinforced composites is considerably important.

Microstructural design is an important approach for enhancing material behavior at the macroscopic scale. Thus, microstructural characterization of composite materials is a necessity for understanding the relationships between microstructural quantities and mechanical properties. For particulate reinforced composite materials, the relevant statistical quantities describing the microstructure include, e.g., spatial distribution and volume fraction of particles. Mechanical properties of particulate reinforced composites are highly dependent on the real microstructure of the composite [15, 20-23], and in this respect, methods capable for accurate quantification of the microstructure across multiple length scales are most desirable. In addition to modelling of the mechanical performance of the material, the results of these measurements can be used, e.g., for quality control and tuning of processing parameters.

X-ray computed tomography (XCT) is a powerful non-destructive method to characterize the structure of heterogeneous materials [24-25]. The method is based on computationally reconstructing the three-dimensional (3D) structure of the sample from a number of two-dimensional X-ray attenuation images taken from different directions [26]. Particularly useful flavor of XCT for materials science is X-ray microtomography, where the resolution of the 3D image is of the order of one micrometer. Such a resolution enables convenient characterization of the overall structure of many kinds of traditional composite materials where the size of the individual reinforcement domains is typically several micrometers. One area attracting a lot of attention is the area of submicron X-ray tomography, popularly dubbed X-ray nanotomography [27]. Recently XCT devices capable of resolutions in the 50 nm range have been introduced [28-29]. In many cases such devices can be used, e.g., to characterize the internal structure of individual reinforcement domains. The downside of increased

resolution is decreased volume of the region visible in the image. Thus, to capture all the relevant structural information, a multiscale characterization is often required.

In XCT studies the information about the structure of the material is in the form of a 3D volume image. In order to arrive in estimates of relevant engineering quantities, like volume fractions and sizes of reinforcement domains, image analysis must be performed. Often such analysis is done manually, but to decrease operator-induced bias and increase the size of data that can be analyzed, automated methods are usually preferred.

XCT has been adopted to characterize the microstructure of various kinds of composite materials [30-32]. For example, Quan et al. [33] characterized the microstructure of additively manufactured parts; Miettinen et al. [34] introduced an automated method to evaluate the fiber length distribution of short-fiber composites from a binarized 3D tomographic image of material sample; and Joffre et al. [35] investigated the fiber length degradation of wood pulp-fiber reinforced polylactide composites by XCT.

In order to exploit the full potential of metallic glass particles in composite materials, better understanding of real morphology of these materials and the effect of processing parameters on the spatial distribution of particles is crucial. In this study, XCT has been used to characterize the 3D distribution of $Ni_{60}Nb_{40}$ particles and clusters in magnesium matrix. This investigation studied the relevant statistical quantities describing the microstructural inhomogeneity of particulate reinforced composites. A method based on X-ray microtomography is presented to measure these quantities. This method is capable of measuring the size distribution of clusters, distribution of distance between clusters and distribution of particle volume fraction inside the clusters. This study provides precise picture of the microstructural heterogeneity in the particulate reinforced composites.

2. Microstructural inhomogeneity parameters

The MMC materials are often fabricated by a powder metallurgy and extrusion process or by liquid infiltration and thus it is difficult to obtain a uniform and homogeneous distribution of reinforcement particles. Thus, some local regions have higher concentration of particles than the average volume fraction in the material. Additionally there may be a tendency for particle clustering, especially in the fabrication processes of real materials, where individual reinforcement particles form agglomerates whose mechanical properties differ from those of individual particles and matrix.

At the largest scale studied here, the local volume fraction and its spatial distribution characterizes the variability of the amount of reinforcement. The amount of clustering can be naturally expressed by dividing the total volume of particles V_f into two parts V_f^c and V_f^m where V_f^c is the volume of clustered particles, V_f^m is the volume of individual particles, and $V_f = V_f^c + V_f^m$. The volume ratio of the particles in the clusters over the total particles, i.e., the fraction of particles in clusters, is then defined as

$$\zeta = \frac{V_f^c}{V_f}. \tag{1}$$

From the point of view of mechanical properties, a particle cluster is effectively the region around a group of agglomerated reinforcement particles where the mechanical properties of the material are different from the surroundings [15]. Denoting that volume by V_{ci} for cluster i, we end up with another natural descriptor of amount of clustering, the volume fraction of clusters

$$\gamma = \frac{V_c}{V}, \tag{2}$$

where $V_c = \sum V_{ci}$ is the total volume of all clusters and V is the total volume of the sample. The local volume fraction of agglomerated reinforcement particles in the volume of the cluster is defined by

$$f_{ci} = \frac{V_f^{ci}}{V_{ci}} \tag{3}$$

where V_f^{ci} is the volume of particles in the cluster and V_{ci} is the volume of the cluster.

3. Materials and methods

3.1. Materials

Amorphous alloy powder with composition $Ni_{60}Nb_{40}$ (at. %) was prepared by mechanically alloying powder mixtures of elemental Ni and Nb metals. The powder mixture was milled at room temperature in air for 87 h, using a Retsch PM400 planetary ball mill with a ball-to-powder ratio of 3:1 and milling speed of 200 rpm. To produce Mg-composites, elemental Mg-powder (99.6% purity) was blended with volume fraction 5% of $Ni_{60}Nb_{40}$ powder for a duration of 1 h and consolidated at room temperature at 450 MPa for 1 min. The compacted cylindrical billets of 36 mm diameter were microwave sintered at 100% power level for 12.5 min so as to achieve a temperature of 550^0C (based on prior calibration). The sintered billets were soaked at 400^0C for 1 h, and hot extruded at 350^0C to produce rods of 8 mm diameter. Rods extruded at 750 psi and 600 psi were used for further analysis.

3.2. X-ray micro- and nanotomography and image analysis

In order to select representative regions of the rods for high-resolution XCT analysis, low-resolution XCT images of the intact rods were captured using SkyScan 1172 microtomograph (Bruker-microCT, Belgium) with 5 μm pixel size. The X-ray tube acceleration voltage and power were set to 100 kV and 5.5 W, respectively, and 1 mm aluminum filter was used in

order to absorb low-energy X-rays not necessary for imaging. 1800 projection images over 360^0 of rotation were acquired with a total of 31 s exposure time per angular position. In the reconstructed volume images, regions containing large amount of reinforcement particles could be easily distinguished from nearly particle free regions (Figure 1). The particles were segmented from the images with simple thresholding such that their average volume fraction in the whole sample became 5 %. Local volume fraction was then determined by local averaging using a window corresponding to the size and shape of the sample in the following high-resolution XCT study described below.

For high-resolution XCT imaging two cylindrical (diameter ≈ 1 mm, height ≈ 1 mm) regions were selected from each rod. One of the regions was taken from a location with low reinforcement concentration (entitled 'normal' region) and the other from a location with high reinforcement concentration (entitled 'clustered' region, see also section 3.1) as shown with red cycle in the Fig. 1. One of the selected regions with low reinforcement concentration is visualized in Fig. 1. Samples corresponding to the selected regions were milled out from the material and glued on the top of sample holder rods. The samples were imaged using Xradia MicroXCT-400 tomograph (Zeiss Xradia, Concord, California, USA) with 0.59 μm pixel size. The X-ray tube voltage and power were 40 kV and 4 W, respectively, and 0.37 mm glass filter was applied. Total of 1800 projection images over 360 degrees of rotation were acquired with 50 s exposure time per angular position.

Segmentation of the reinforcement regions in the reconstructed high-resolution images was made using local thresholding with Phansalkar method [36]. The segmented regions were classified into clustered and individual particles based on observation that a cluster consisting of multiple smaller particles has many local gray-value maxima inside it, even though the

individual particles forming the cluster may not be distinguishable from each other. Thus, a reinforcement region was classified as a cluster of particles if the original volume image contained more than three local maxima in the corresponding region; otherwise, the region was classified as an individual particle. This classification resulted in visually plausible results irrespective whether the sample was taken from region with high or low reinforcement concentration (Figure 2a-d).

In order to determine the microstructural inhomogeneity parameters ζ and γ, one must calculate the volume of particles V_f, the volume of particles in clusters V_f^c, the volume of the composite V, and the volume of particle clusters V_c. The volume of particles and the volume of particles in clusters were determined as the count of pixels in all particles, and count of pixels in regions classified as particle clusters, respectively. The volume of composite was determined by manually measuring the size of the sample in the image.

The volume V_c refers to the total volume of regions around clusters where the elastic properties of the material are different from the non-clustered surroundings. Such a volume cannot be directly seen in the XCT images and thus geometric approximation must be done instead. Here we propose two approaches for approximating V_c, viz. bounding spheres of clusters [15] and bounding ellipsoids of clusters. The bounding sphere for each cluster, i.e. the smallest sphere that contains all the cluster pixels, was determined using Welzl method [37] that calculates the optimal bounding sphere of a set of points in linear time using a randomized linear programming type algorithm.

The bounding ellipsoid for a cluster was determined using principal component analysis (PCA) [38]. The directions of the semi-axis of the bounding ellipsoid were taken to be the

three principal components of the cluster pixels. The lengths of the semi-axis were selected to be square roots of variances in the directions corresponding to the principal components, scaled uniformly such that all the cluster pixels fit into the ellipsoid.

Finally, the volume of bounding spheres (ellipsoids) was determined as the count of pixels inside at least one of the bounding spheres (ellipsoids), and the results were used to determine two sets of microstructural parameters, one for spherical and one for ellipsoidal clusters.

In order to determine inner diameter of clusters (see Fig. 3), the local thickness algorithm was used [39]. It replaces value of each pixel in the image by the diameter of the largest sphere that fits into the cluster and contains the pixel. The sphere is considered to fit into the cluster if there are no background pixels inside the sphere. The distribution of cluster diameter was then calculated by statistical binning of the pixel values in the image. The distribution of distance between clusters was determined similarly but by applying the local thickness algorithm to the background between the clusters.

In order to characterize the internal structure of particle clusters and measure the amount of very small reinforcement particles that are not seen in the microtomographic images, regions around randomly selected particle clusters were imaged with Xradia nanoXCT-100 device. The device employs X-ray optics optimized for 8 keV photons to focus a magnified X-ray projection image of the sample on a camera. In order to make a tomographic scan, 901 projection images with 65 nm pixel size were recorded over 180 degrees of rotation. Exposure time for single projection image was 200 s. The reconstructed volume images (see Figure 1d) were processed similarly to the microtomographic images discussed above, except thresholding was done with Otsu method [40] after Gaussian smoothing ($\sigma = 65$ nm).

4. Results and discussion

The applicability of the developed method based on X-ray tomography is investigated in multi-scale microstructural characterization of particulate reinforced MMCs, extruded at different pressure loads.

4.1. Internal structure of individual clusters and X-ray nanotomography

The structure of individual clusters in the 5 vol. % $Ni_{60}Nb_{40}$/Mg composites was probed with X-ray nanotomography as discussed in section 3-2. Figures 1c-d and 4 shows nanotomographic slices through, and 3D visualizations of two particle clusters taken from rods extruded at different pressure loads. The cluster extruded at 600 psi seems to be solid and relatively spherical when compared to the cluster extruded at 750 psi. The latter one consists of multiple small pieces of reinforcement that have been broken, possibly during the extrusion process. This suggests that there may be two types of clusters in the present composites; intact, relatively spherical ones and broken, more ellipsoidal ones. This conclusion is supported by Figure 4b, where the local inner diameter distributions of the two clusters are shown. The diameter distribution of the cluster extruded at 600 psi exhibits a large peak with small background, corresponding to almost spherical structure. The distribution for the cluster extruded at 750 psi displays several peaks, corresponding to a more complicated structure with several, almost separate, parts.

In order to model the effect of clusters on the mechanical properties of the material, homogenization techniques may be used to convert the complicated cluster structure into an equivalent inclusion (see Eq. 3). In this process, the volume fraction of particles inside the cluster, f_{ci} is one of the governing parameters, in addition to the shape of the cluster. The Table 1 shows volume fractions of particles inside the clusters in the nanotomographic

images, for both ellipsoidal and spherical bounding volumes as discussed in section 3-2. In this table, $V_{c,ball}/V_{c,ellipsoid}$ shows the degrees of freedom in bounding with a sphere compare to an ellipsoid. The results indicate that for the spherical cluster in the sample extruded at 600 psi pressure load the two methods give similar values for f_{ci}, but for the more complicated cluster structure in the sample extruded at 750 psi pressure the results corresponding to the two techniques differ more.

The nanotomographic images can also be used for verification of results calculated from the microtomographic images below. To this end, the resolution of the nanotomographic images was artificially reduced such that it corresponded to the resolution of the microtomographic images. The particle cluster and individual particles were then analyzed from both the reduced-resolution and the full-resolution images as discussed in section 3-2. Comparison of the results indicates that the difference in volume of individual particles is on average 3.7 % between the full resolution images and the reduced resolution images. The corresponding difference in cluster volume is on average 0.5 %. The relatively small differences suggest that the resolution of the microtomographic images is good enough for the analysis presented below.

Material		f_{ball}^{ci}	$f_{ellipsoid}^{ci}$	$V_{c,ball}/V_{c,ellipsoid}$
5. vol%	600 psi	0.38	0.35	0.92
	750 psi	0.13	0.27	2.07

Table 1. Volume ratio and local volume fraction of different fitting approaches.

4.2. Microstructural inhomogeneity parameters

Figure 5 shows the microstructural inhomogeneity parameters, ζ and γ, of 5 vol. % $Ni_{60}Nb_{40}$/Mg composites for regions with low and high concentration of particles. These

parameters have been calculated from the microtomographic images based on the method and definition discussed in section 3-2 for spherical and ellipsoidal clusters. The specimens have been chosen from different rods extruded at 600 psi and 750 psi. The values of the inhomogeneity parameters are lower for regions with low concentration of reinforcement, revealing that the microstructure of the material differs between locations. Locations with low concentration of reinforcement are thus not as clustered as locations with high concentration of reinforcement. This observation is consistent with Fig. 2, where the locations with high concentration of particles exhibit visually more clustering, and suggests that the elastic behavior of the material is different from region to region.

It can be seen that the specimen with higher extrusion load has lower values for the clustering parameters. This means smaller amount of particles are agglomerated in the clusters and the volume fraction of clusters is lower. Moreover, Figure 5 indicates that the volume fraction of clusters, γ, possess higher values for bounding spheres approach compared to the bounding ellipsoids approach

The microstructural inhomogeneity parameters can be used both as an indicator of processing conditions during manufacturing and of mechanical properties of the product. As an example, the results of measurements of Young's modulus and tensile properties of these composite materials are listed in Table 2. Increase in γ and ζ means volume fraction of clusters increase while larger amount of particles are agglomerated in the clusters. This implies that the local rigidity is increased in the material. In this respect, the agglomeration degree of particles is higher and the clustered regions will be potential sites for damage formation. However, this aspect should be investigated in more detail and thus the effects of clustering and critical

microstructural characteristics of particulate reinforced composite on damage formation will be further investigated in the following part of this study.

Material		Young's modulus (GPa)	0.2% Offset Yield Strength (MPa)	Tensile Strength (MPa)	ζ_{normal}	γ_{normal}	$\zeta_{cluster}$	$\gamma_{cluster}$
5. vol%	600 psi	40.7	84	109	0.90	0.08	0.96	0.47
	750 psi	46.5	174	208	0.51	0.02	0.84	0.32

Table 2. Results of room temperature tensile testing [15] and clustering parameters.

4.3. Cluster size

The importance of reducing the cluster size is critical if particulate reinforced metal matrix composites are to compete with monolithic alloys, e.g., in automotive and aerospace structural applications. In these applications, tensile strength and fatigue behavior are critical material selection drivers, and both properties are adversely affected by particle clustering [15,19]. Figures 6a-b depict the distribution of particle volume and cluster diameter of 5 vol. % $Ni_{60}Nb_{40}$/Mg composites in various locations with different microstructures. In the case of normal region for composite extruded at 750 psi, peak in the probability density of cluster diameter (which corresponds to the most probable cluster sizes) occur at values lower than in the composite extruded at lower load. The peak is also higher and narrower than for composite extruded at 600 psi, indicating a larger size concentration in smaller range of diameters. Moreover, it can be seen that the particle volume and cluster size distribution of composites extruded at 600 psi do not vary considerably with respect to region. Additionally, they have a similar variation; however, this trend is quite different in the case of composite extruded at higher load. Indeed, in terms of particle volume and diameter, clustered region in

composite extruded at 750 psi corresponds well to both normal and clustered regions in composite extruded at 600 psi. The same correspondence can be seen also in the visualizations in Figure 2.

4.4. Cluster distance

When multiple clustered reinforcement regions are in close proximity, they behave as a large single cluster. Thus, it is important to elucidate the effects of processing parameters on the proximity of clusters. Figure 7 shows the distribution of distance between clustered particles of 5 vol. % $Ni_{60}Nb_{40}$/Mg composites in various locations with different reinforcement concentration. It is apparent that the distribution is shifted towards large distances between clusters in the normal regions. In addition to smooth background, the distributions exhibit sharp local maxima. Each of those corresponds to one or more large, cluster-free regions of the same diameter, and they seem to occur more frequently in the composite extruded at 750 psi than in the composite extruded at 600 psi. The peaks are higher for normal region of the composite extruded at 750 psi than for normal region of the composite extruded at 600 psi, implying that large, cluster-free regions constitute a larger fraction of the total cluster-free volume in the sample extruded at 750 psi.

4.5. Volume fraction of particles in clusters

The volume fraction of particles inside each cluster, f_{ci}, is determined to make a more accurate characterization of the microstructural heterogeneity. The volume of particles inside each cluster, V_f^{ci}, is determined as total count of pixels in each individual cluster. The volume of each cluster, V_{ci}, is calculated using Welzl algorithm for bounding spheres and PCA algorithm for bounding ellipsoids of the cluster as explained in section 3-2.

Figures 8a-b, 9a-b show the bivariate distributions of particle volume fraction inside the clusters and volume of individual clusters using sphere bounding and ellipsoid bounding approach, respectively, for normal region of 5 vol. % $Ni_{60}Nb_{40}$/Mg composites extruded at 750 psi and 600 psi. Figures 10a-b, and 11a-b show the same distributions for clustered region. It can be seen that smaller clusters have large variety of particle volume fraction. In the normal region chosen from the rod extruded at 600 psi, count of clusters with high concentration of particles is greater than in normal region of rod extruded at 750 psi, which is not desirable. The clustered regions have higher rigidity due to high Young's modulus of particles and they seem to be the fracture origins and potential sites for interface debonding and crack formation [15]. Therefore, it is preferable to have clusters with low concentration of particles than clusters with high concentration of particles. By comparing Figures 9 and 8, it can also be concluded that extruding at 750 psi decreases count of large clusters and increases count of small clusters.

Figures 12a-b depict the distribution of particle volume fraction inside the clusters using sphere bounding and ellipsoid bounding approach, respectively, for different microstructures of 5 vol. % $Ni_{60}Nb_{40}$/Mg composites (i.e. marginal distributions of the bivariate distributions in Figs. 8-11). Smaller volume fractions are more probable than the larger ones as seen particularly by the rather early peak in data corresponding to the normal region of the composite extruded at higher load. The peak is found to be highest at low values of local volume fraction signaling a preponderance of relatively sparse cluster regions.

Conclusions

Methods for characterization of the particulate reinforcement distribution in MMCs using 3D X-ray micro- and nano-tomographic images were developed. The tomographic images of composite materials and microstructural inhomogeneity parameters calculated based on the images were used in finding critical morphological characteristics of particulate reinforced composites. The images revealed that on the largest scale studied, the spatial distribution of reinforcement in the composite material is very uneven. On intermediate scale there seems to be multiple types of microstructures: the regions with low volume fraction of reinforcement contain less particle clusters than the regions with high concentration of particles. Furthermore, X-ray nanotomography suggests that the structure of the individual clusters of reinforcement particles vary from regular, solid ones to highly irregular, broken ones. This might be due to higher extrusion load causing larger forces that break regular particles into irregular ones, but confirmation of such a hypothesis would require more experiments.

The results indicate that the microstructural inhomogeneity parameters vary in different locations in the material. These parameters possess lower values in the regions with low concentration of reinforcement while their values increase significantly in the regions with high concentration of particles. Moreover, these parameters can be used as an indicator of processing conditions during manufacturing as they possess lower values for composites extruded at higher pressure loads.

It was also shown that the composite extruded at higher load exhibits more cluster-free regions and overall size of clusters is smaller than in composite extruded at lower load. Additionally, extruding at lower load seems to lead to more clusters with high volume fraction of particles. These trends are the same irrespective whether the total volume of a

cluster is defined using bounding sphere or bounding ellipsoid, although nanotomographic imaging suggests that bounding ellipsoids may lead to much smaller (i.e. better fitting) bounding volumes.

This study confirms multi-scale 3D imaging as a powerful quantification method for microstructural characterization allowing inhomogeneity parameters to be defined to study the effects of processing parameters on the spatial distribution of the reinforcement particles and their critical morphological characteristics. Results and techniques discussed here will be applied in modelling of the MMC materials in part II of this study.

References

[1] Miracle DB. Metal matrix composites – from science to technological significance. Compos Sci Technol 2005;65:2526–40.

[2] Gupta M, Nai SML. Magnesium, magnesium alloys and magnesium composites. New Jersey: John Wiley & Sons; 2011.

[3] Garces G, Rodriguez M, Perez P, Adeva P. Effect of volume fraction and particle size on the microstructure and plastic deformation of Mg–Y_2O_3 composites. Mater Sci Eng A 2006;419:357–64.

[4] Garc´es G, P´erez P, Adeva P. Effect of the extrusion texture on the mechanical behavior of Mg–SiCp composites. Scripta Mater 2005;52:615–19.

[5] Jayalakshmi S, Zhenhua L, Sankaranarayanan S, Hamouda AS, Gupta M. Microstructure and mechanical properties of Mg–5Nb metal–metal composites reinforced with nano-SiC ceramic particulates. Metal 2012;2:178–84.

[6] Jayalakshmi S, Quy Bau N, Gupta M. Effect of Cr addition and carbon dioxide incorporation during processing on the microstructural and mechanical properties of AZ31 magnesium alloy. Mater Chem Phys 2012;134:721–7.

[7] Sankaranarayanan S, Jayalakshmi S, Gupta M. Effect of individual and combined addition of micro / nano-sized metallic elements on the microstructure and mechanical properties of pure Mg. Mater Des 2012;37:274–84.

[8] Scudino S, Liu G, Prashanth KG, Bartusch B, Surreddi KB, Murty BS, et al. Mechanical properties of Al-based metal matrix composites reinforced with Zr-based glassy particles produced by powder metallurgy. Acta Mater 2009;57:2029–2039.

[9] Dudina DV, Georgarakis K, Li Y, Aljerf M, LeMoulec A, Yavari AR, et al. A magnesium alloy matrix composite reinforced with metallic glass. Compos Sci Technol 2009;69:2734–2736.

[10] Kim JY, Scudino S, Kühn U, Kim BS, Lee MH, Eckert J. Production and characterization of brass-matrix composites reinforced with Ni59Zr20Ti16Si2Sn3 glassy particles. Metals 2012;2:79–84.

[11] Jayalakshmi S, Gupta S, Sankaranarayanan S, Sahu S, Gupta M. Structural and mechanical properties of Ni60Nb40 amorphous alloy particle reinforced Al-based composites produced by microwave–assisted rapid sintering. Mater Sci Eng A 2013;518:119–127.

[12] Sankaranarayanan S, Hemanth Shankar V, Jayalakshmi S, Bau NQ, Gupta M. Development of high performance magnesium composites using Ni50Ti50 metallic glass reinforcement and microwave sintering approach. J Alloys Compd 2015;627:192–199.

[13] Hong S-J, Kim H-M, Huh D, Chun BS, Suryanarayana C. Effect of clustering on the mechanical properties of SiC particulate-reinforced aluminum alloy 2024 metal matrix composites. Mater Sci Eng A 2003;347(1–2):198–204.

[14] Conlon K.T., Wilkinso D.S. Effect of particle distribution on deformation and damage of two-phase alloys. Mater Sci Eng A 2001;317:108–114.

[15] Nafar Dastgerdi J, Marquis G, Anbarlooie B, Sankaranarayanan S, Gupta M, Microstructure-sensitive investigation on the plastic deformation and damage initiation of amorphous particles reinforced composites, Compos Struct 2016;142:130-139.

[16] Murphy AM, Howard SJ, Clyne TW. Characterisation of severity of particle clustering and its effect on fracture of particulate MMCs. Mater Sci Techno 1998;14:959–68.

[17] Kumai S., Hu J., Higo Y., Nunomura S. Effect of dendrite cell size and particle distribution on the near-threshold fatigue crack growth behavior of cast Al-SiCp composites. Acta. mater. 1996;44: 2249–57.

[18] Lorca J. Fatigue of particle and whisker- reinforced metal matrix composite. Prog. Mater. Sci. 2002;47:283-353.

[19] Nafar Dastgerdi J, Marquis G, Sankaranarayanan S, Gupta M, Fatigue crack growth behavior of amorphous particulate reinforced composites. Compos Struct 2016;153:782-790.

[20] Segurado J., Llorca J. Computational micromechanics of composites: The effect of particle spatial distribution Mech.Mater. 2006;38:873–883.

[21] Ayyar A., Crawford G.A., Williams J.J., Chawla N. Numerical simulation of the effect of particle spatial distribution and strength on tensile behavior of particle reinforced composites. Comput Mater Sci. 2008;44:496–506.

[22] Peng Z., Fuguo L. Effects of Particle Clustering on the Flow Behavior of SiC Particle Reinforced Al Metal Matrix Composites. Rare Metal Mat Eng. 2010;39: 1525−1531.

[23] Nafar Dastgerdi J, Anbarloei B, Marzban S, Marquis G, Mechanical and real microstructure behavior analysis of particulate-reinforced nanocomposite considering debonding damage based on cohesive finite element method. Compos Struct 2015;122:518-525.

[24] Babout L, Maire E, Buffiere JY, Fougeres R. Characterization by X-ray computed tomography of decohesion, porosity growth and coalescence in model metal matrix composites. Acta Mater 2001;49:2055-2063.

[25] Salvo L, et al. X-ray micro-tomography an attractive characterisation technique in materials science. Nucl Instr Meth Phys Res B 2003;200:273–286.

[26] Withers P. X-ray nanotomography. Mater Today 2007;10 (12):26-34.

[27] Kak AC, Slaney M. Principles of computerized tomographic imaging. IEEE Press; 1988.

[28] Boever WD, et al. Characterization of composition and structure of clay minerals in sandstone with ptychographic X-ray nanotomography. Appl Clay Sci 2015; 118:258-264.

[29] Allahkarami M, Bandla S, Winarski RP, Hanan JC. X-ray nanotomography of a nanofiber: Quantitative measurement of diameter fluctuations. Appl Surf Sci 2014;297:9-15.

[30] Luengo Hendriks CL. Constrained and dimensionality-independent path openings. IEEE Trans Image Process 2010;19 (6):1587–95.

[31] Maire E, Withers PJ, Quantitative X-ray tomography. Int Mater Rev 2014:59(1):1-43.

[32] Tammas-Williams S, Zhao H, Leonard F, Derguti F, Todd I, Prangnell PB, XCT analysis of the influence of melt strategies on defect population in Ti-6Al-4V components manufactured by Selective Electron Beam Melting, Mater Charact 2015;102:47-61.

[33] Quan Z, Larimore Z, Qin X, Yu J, Mirotzink M, Byun JH, Oh Y, Chou TW. Microstructural characterization of additively manufactured multi-directional performs and composites via X-ray microcomputed tomography. Compos Sci Technol 2016;131:48-60.

[34] Miettinen A, Luengo Hendriks C, Chinga-Carrasco G, Gamstedt E, Kataja M. A non-destructive X-ray microtomography approach for measuring fibre length in short-fibre composites. Compos Sci Technol 2012;72(13):1901–8.

[35] Joffre T, Miettinen A, Berthold F, Gamstedt EK. X-ray micro-computed tomography investigation of fibre length degradation during the processing steps of short-fibre composites. Compos Sci Technol 2014;105:127–33.

[36] Phansalkar N. et al. Adaptive local thresholding for detection of nuclei in diversity stained cytology images. International Conference on Communications and Signal Processing (ICCSP) 2011, 218-220.

[37] Welzl E. Smallest enclosing disks (balls and ellipsoids), New Results and New Trends in Computer Science (H. Maurer, Ed.), Lecture Notes in Computer Science 1991;555:359-370.

[38] Pearson K. On lines and planes of closest fit to systems of points in space. Philosophical Magazine 1901;2:559–572,.

[39] Hildebrand T, Rüegsegger P. A new method for the model-independent assessment of thickness in three-dimensional images. Journal of Microscopy 1997;185(1):67–75,.

[40] Otsu N, A threshold selection method from gray-level histograms, IEEE Trans Syst Man Cybernet 1979;9:62–66.

Figure 1

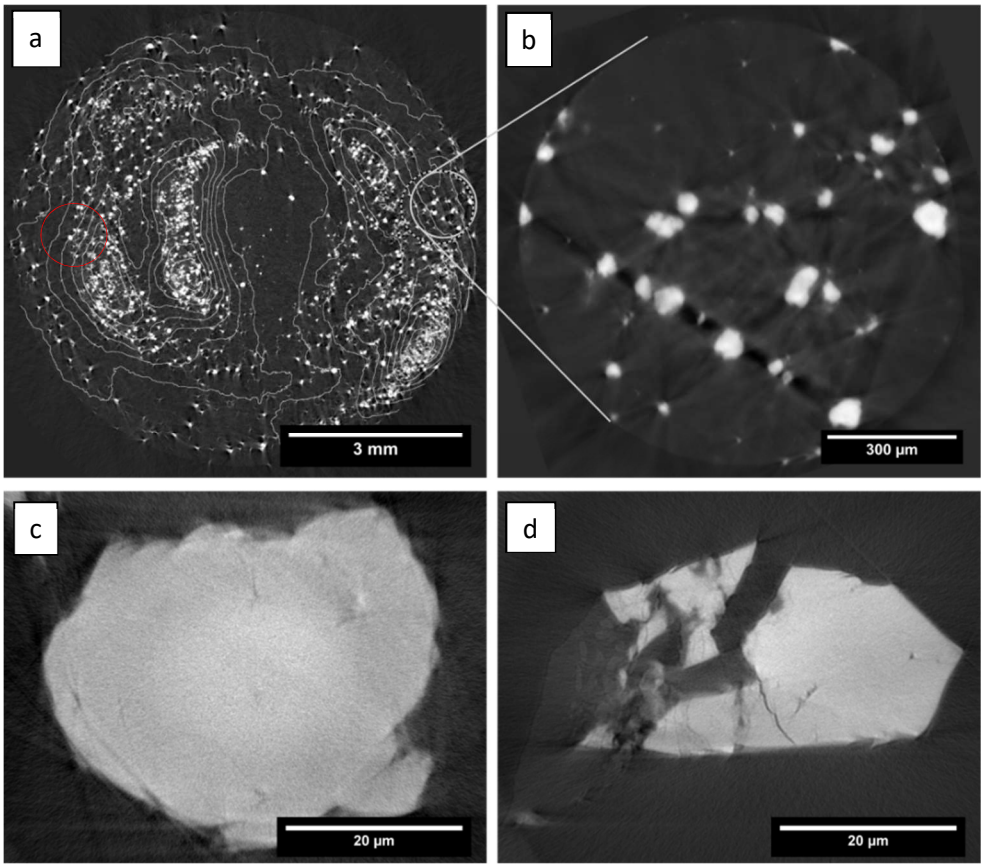

Figure 1. (a) Slice through low-resolution XCT image of the sample extruded at 600 psi. The bright dots are the reinforcement particles or particle clusters and the gray curves are contours of local volume fraction field. Dashed circle indicates the intended location of the high-resolution XCT sample, and solid circle indicates its true location as determined with digital image correlation. (b) Slice through a high-resolution XCT image of the region indicated in (a). (c) and (d) Slice through a nanotomographic image of a randomly selected particle cluster in a sample extruded at 600 psi and 750 psi, respectively.

Figure 2

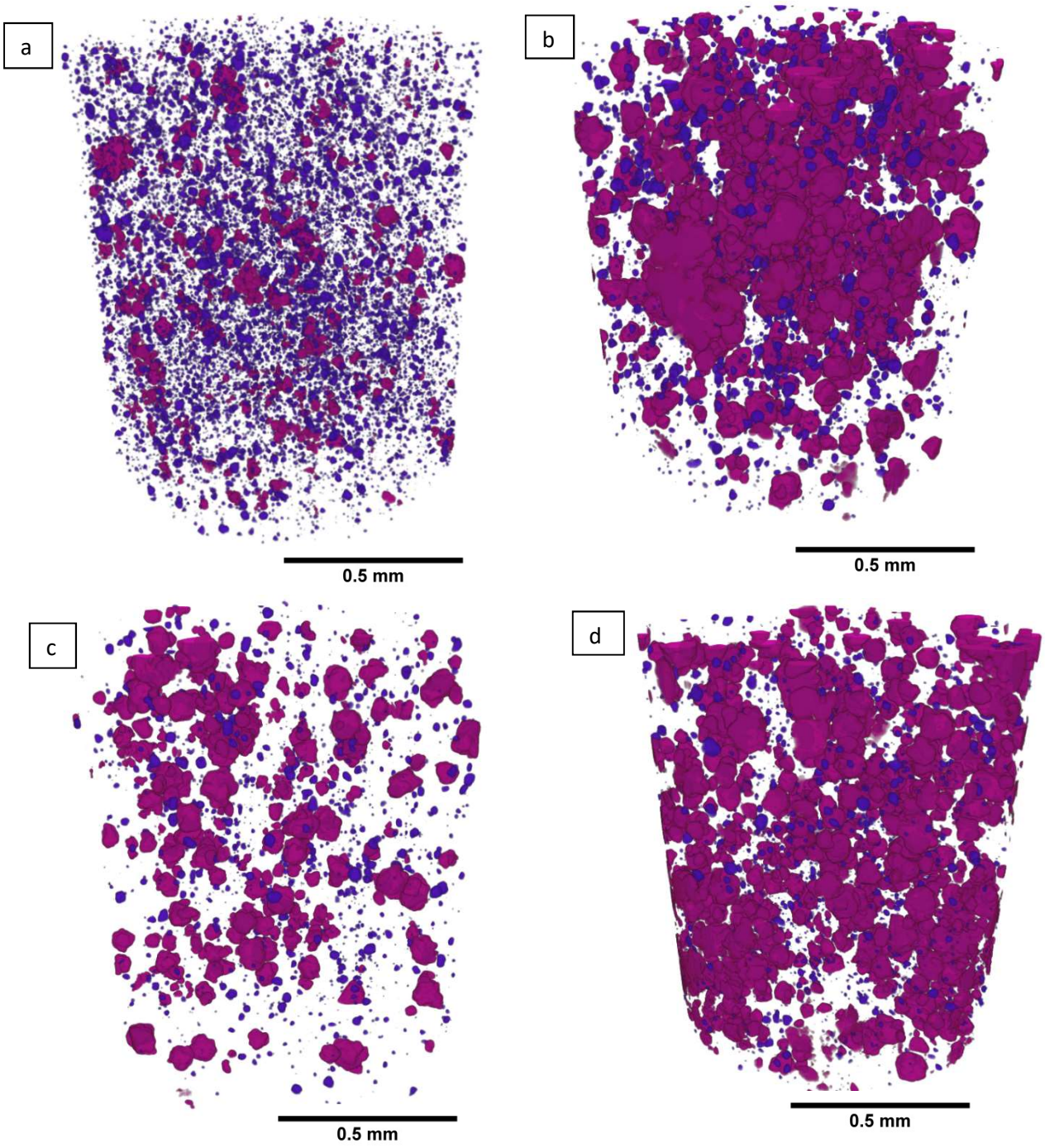

Figure 2. Visualizations of different types of microstructure. (a-b) and (c-d): normal and clustered regions of composite extruded at 750 psi and 600 psi, respectively. Red and purple colors correspond to clustered and individual particles, respectively.

Figure 3

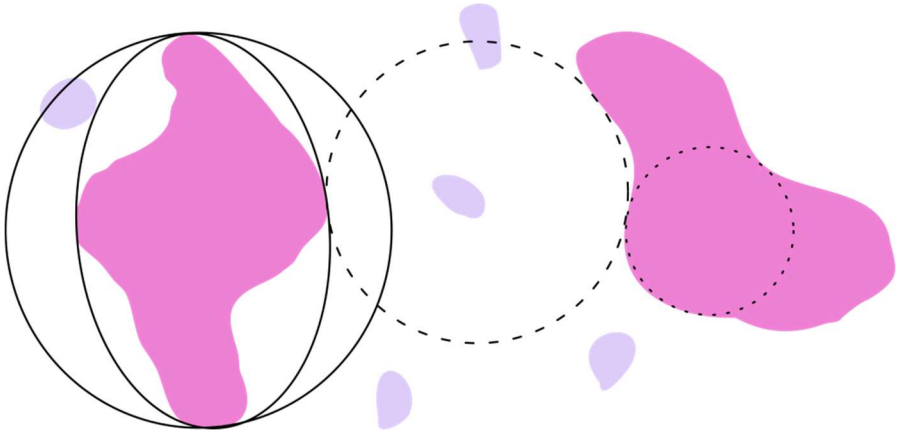

Figure 3. Schematic representation of various diameters measured from the tomographic images. Red and purple regions represent clustered particles and individual particles, respectively. Solid circle and solid ellipse represent bounding volumes of the cluster inside them. Diameter of the dashed circle is the distance between clusters at locations inside the circle. Similarly, the diameter of the dotted circle is the inner diameter of the corresponding cluster at locations inside the circle.

Figure 4

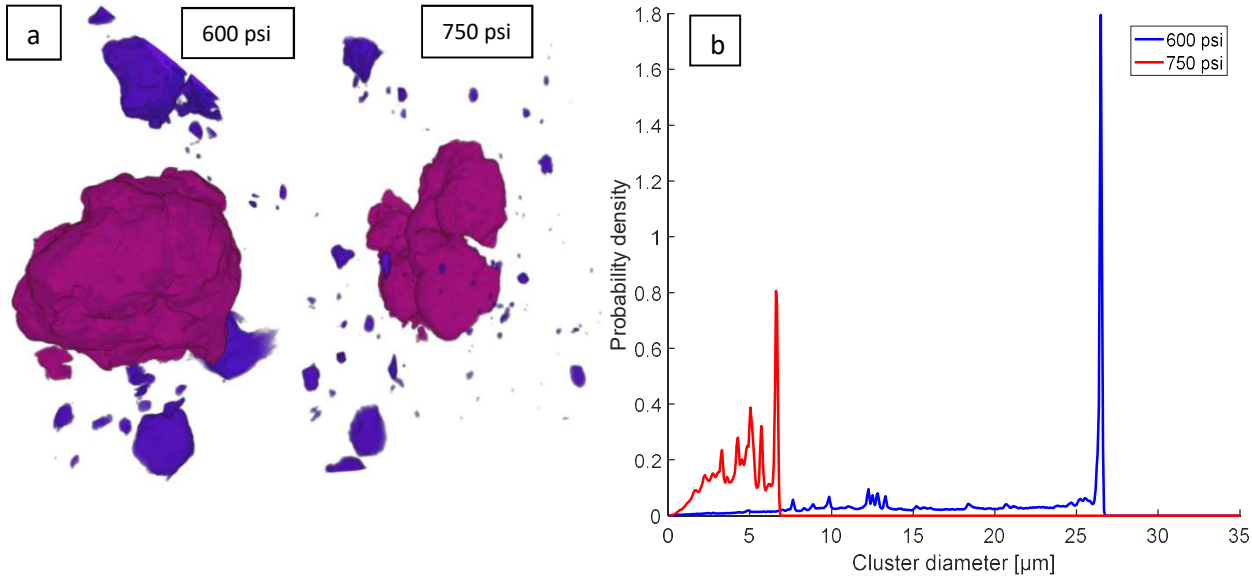

Figure 4. (a) Visualization and (b) diameter distribution of two individual clusters in nanotomographic images. In the visualization at left, the clustered particles are marked with red color and individual particles with purple color.

Figure 5

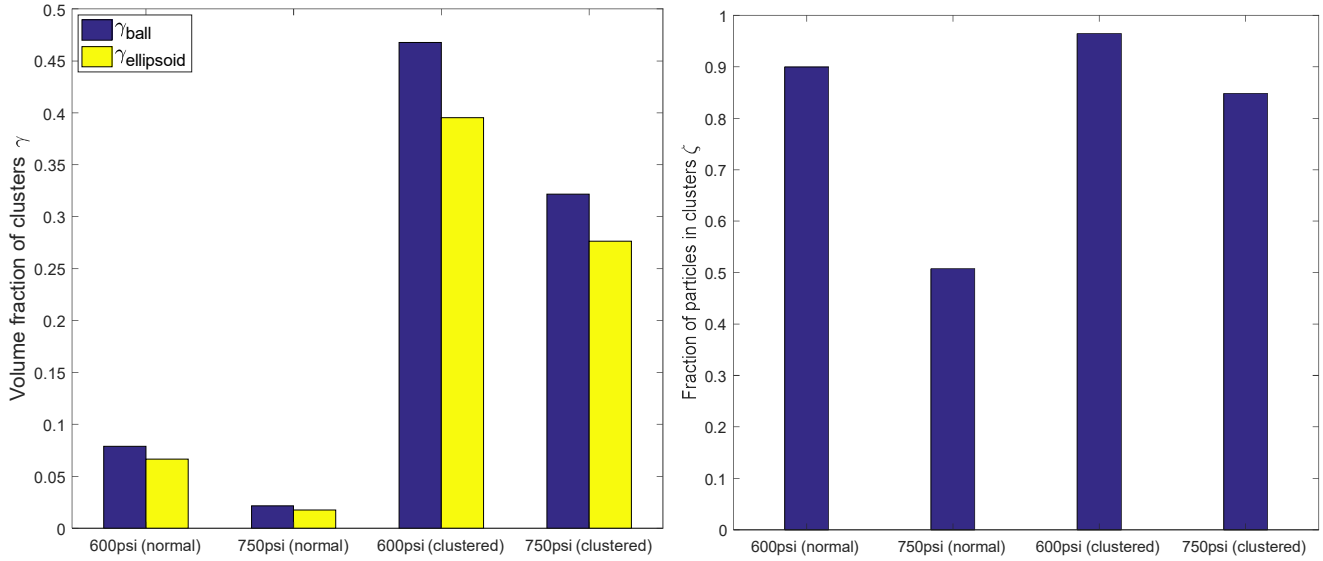

Figure 5. The microstructural inhomogeneity parameters of different types of microstructure (normal and clustered) for samples extruded at different pressure loads.

Figure 6

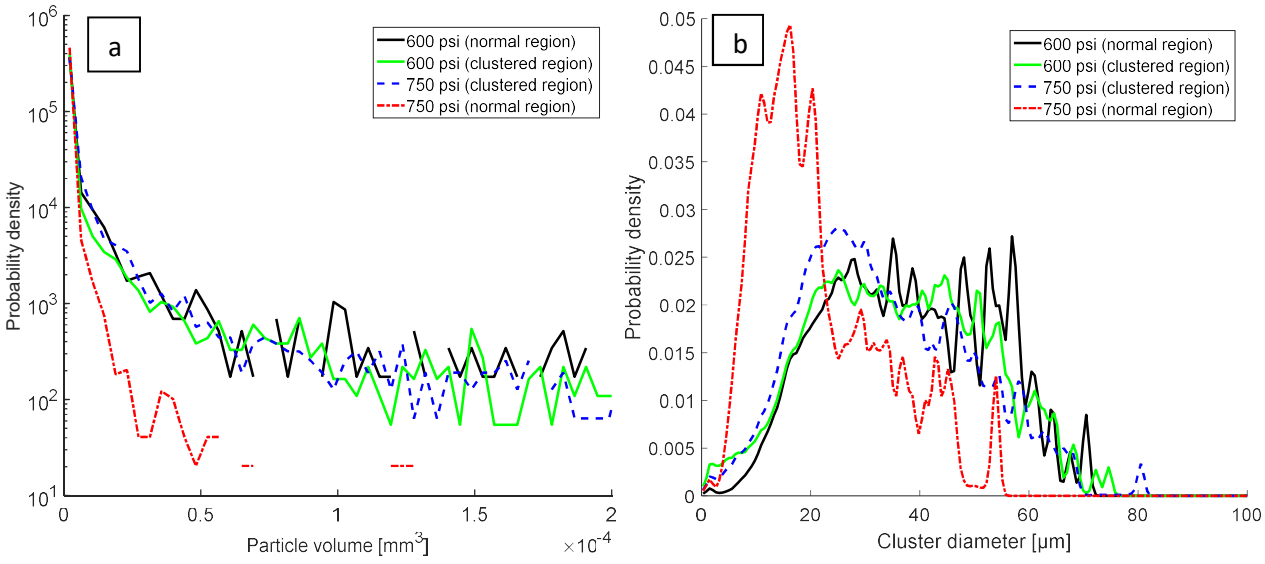

Figure 6. (a) Particle volume and (b) cluster diameter distribution of 5 vol. % $Ni_{60}Nb_{40}$/Mg composites in various regions with different microstructures.

Figure 7

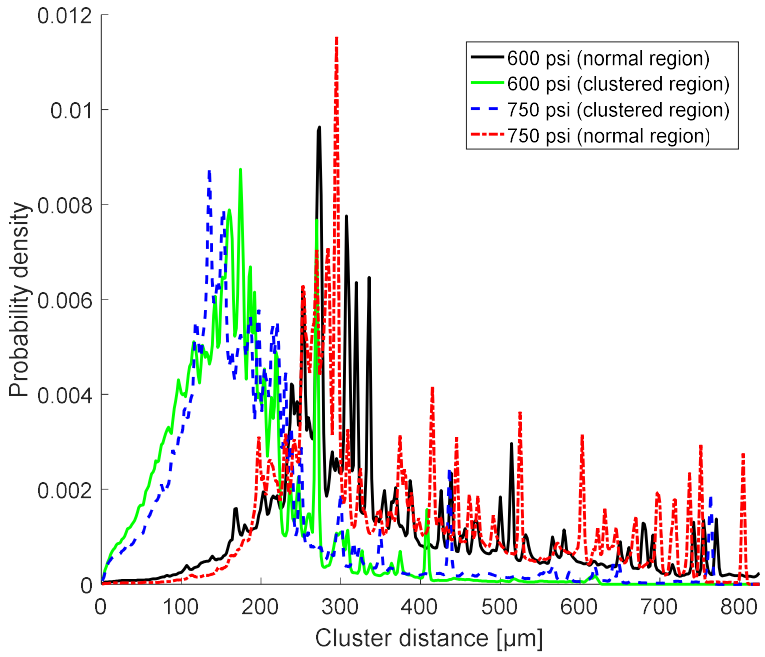

Figure 7. The distribution of distance between clusters of 5 vol. % $Ni_{60}Nb_{40}$/Mg composites with different microstructures.

Figure 8

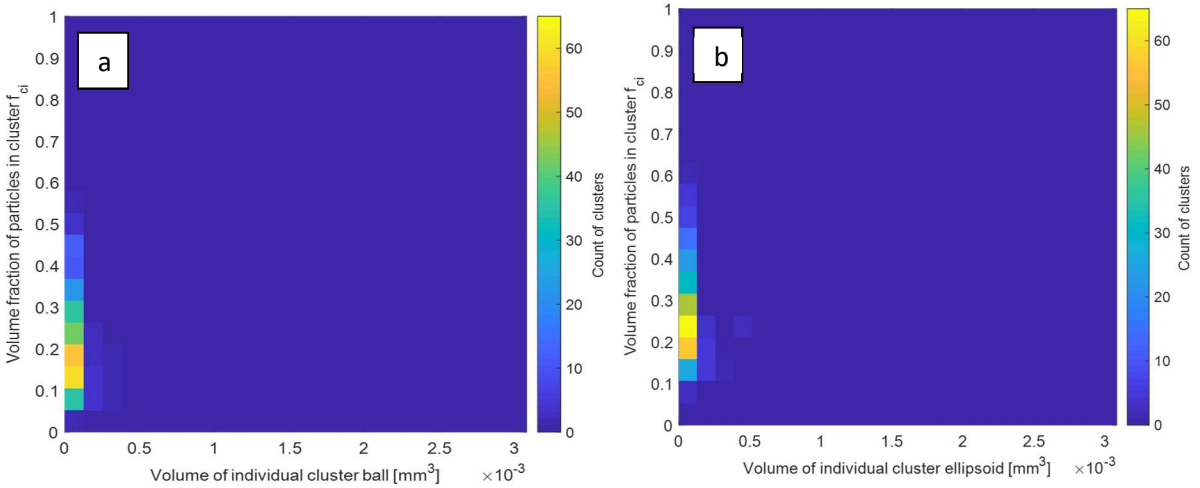

Figure 8. The bivariate distribution of particle volume fraction inside the clusters and volume of individual clusters using (a) sphere and (b) ellipsoid bounding approach in the normal region of composite extruded at 750 psi.

Figure 9

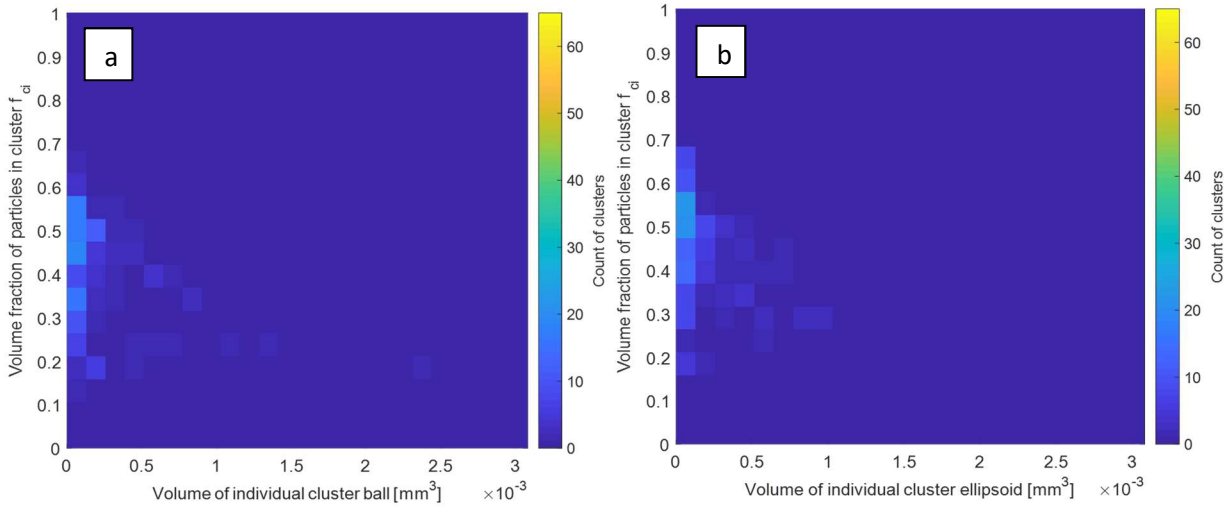

Figure 9. The bivariate distribution of particle volume fraction inside the clusters and volume of individual clusters using (a) sphere and (b) ellipsoid bounding approach in the normal region of composite extruded at 600 psi.

Figure 10

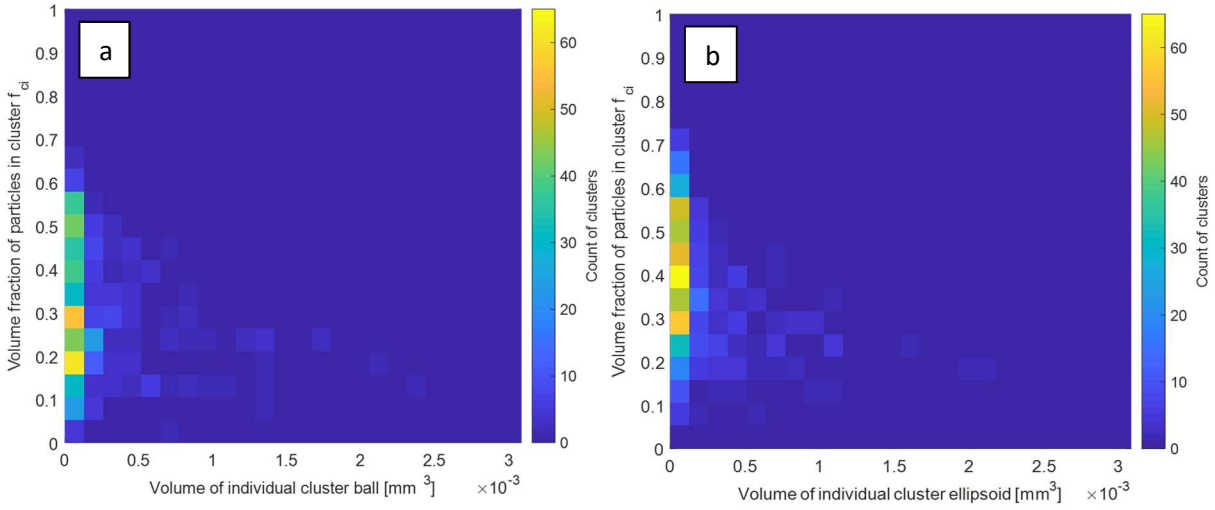

Figure 10. The bivariate distribution of particle volume fraction inside the clusters and volume of individual clusters using (a) sphere and (b) ellipsoid bounding approach in the clustered region of composite extruded at 750 psi.

Figure 11

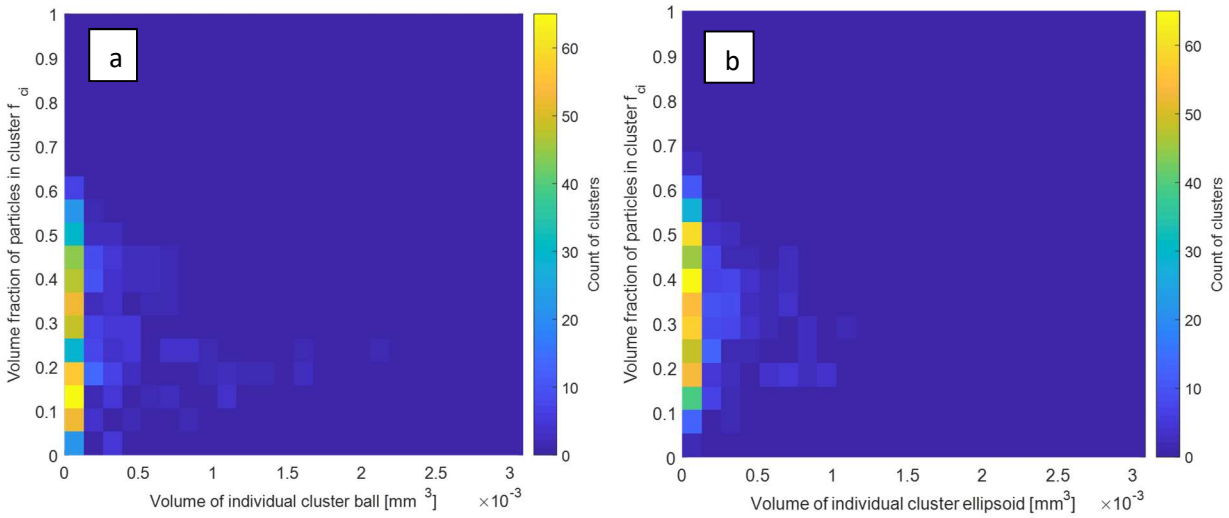

Figure 11. The bivariate distribution of particle volume fraction inside the clusters and volume of individual clusters using (a) sphere and (b) ellipsoid bounding approach in the clustered region of composite extruded at 600 psi.

Figure 12

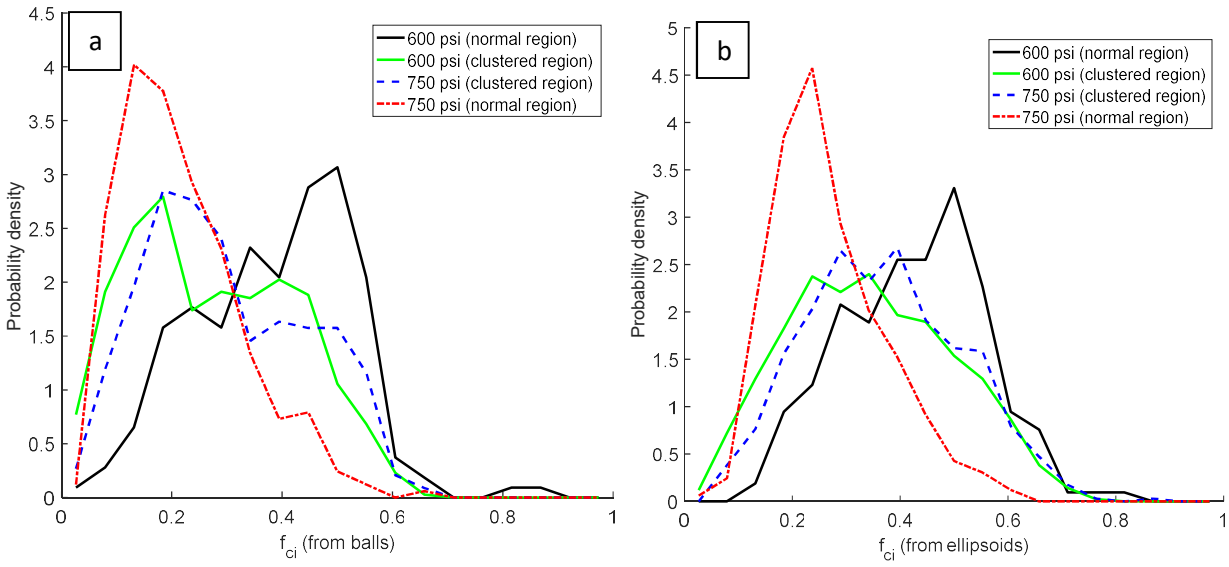

Figure 12. The distribution of particle volume fraction inside the clusters: (a) sphere bounding approach, (b) ellipsoid bounding approach.